


Spatial Coherence of Spin-Orbit-Coupled Bose Gases

Andika Putra,¹ F. Salces-Cárcoba^{1b},¹ Yuchen Yue^{1b},¹ Seiji Sugawa^{1b},^{2,3} and I. B. Spielman^{1b}
¹*Joint Quantum Institute, National Institute of Standards and Technology, and University of Maryland, Gaithersburg, Maryland 20899, USA*

²*PRESTO, Japan Science and Technology, Tokyo 102-0076, Japan*

³*Graduate School of Science, Kyoto University, Kyoto 606-8502, Japan*

 (Received 15 October 2019; accepted 7 January 2020; published 6 February 2020)

Spin-orbit-coupled Bose-Einstein condensates (SOBECs) exhibit two new phases of matter, now known as the stripe and plane-wave phases. When two interacting spin components of a SOBEC spatially overlap, density modulations with periodicity given by the spin-orbit coupling strength appear. In equilibrium, these components fully overlap in the miscible stripe phase and overlap only in a domain wall in the immiscible plane-wave phase. Here we probe the density modulation present in any overlapping region with optical Bragg scattering and observe the sudden drop of Bragg scattering as the overlapping region shrinks. Using an atomic analog of the Talbot effect, we demonstrate the existence of long-range coherence between the different spin components in the stripe phase and surprisingly even in the phase-separated plane-wave phase.

DOI: [10.1103/PhysRevLett.124.053605](https://doi.org/10.1103/PhysRevLett.124.053605)

Systems with coexisting order parameters, such as ferromagnetic superconductors [1], supersolids [2], or topological Kondo insulators [3], exhibit rich phases with novel phenomena. Spin-orbit-coupled Bose-Einstein condensates (SOBECs) have a complex phase diagram including both “stripe” and “plane-wave” phases. The stripe phase is expected to have coexisting order parameters [4–6] with supersolidlike properties [7] marked by long-range phase coherence and periodic density modulations (confirmed by optical Bragg scattering [8]) simultaneously present. In contrast, the plane-wave phase behaves like a ferromagnetic spinor Bose-Einstein condensate (BEC), where its true many-body ground state is predicted to be massively entangled with application to precision magnetometry [9,10]. In both the stripe and plane-wave phases, we readout a matter wave Talbot interferometer with optical Bragg scattering to detect coexisting periodic density modulations (long-range diagonal order) and system-wide phase coherence (long-range off-diagonal order). Unexpectedly, both phases exhibit both types of order.

Figure 1(a) schematically depicts the stripe and plane-wave phases of SOBECs, showing two salient features [5,6,11]: (1) system-wide periodic density modulations are associated with fully coexisting spin components in the stripe phase, and (2) highly localized density modulations

are present at a domain-wall delineating phase-separated spin components in the plane-wave phase. Initial experiments with Raman coupled ⁸⁷Rb Bose-Einstein condensates (BECs) identified these phases in terms of the degree of spatial overlap of the two spin components [5], but not the microscopic density modulations. Direct observation of these modulations in ⁸⁷Rb BECs is challenging both because the ≈ 400 nm modulation period is below the resolution of even the best quantum gas microscope [12] and the modulation contrast is small. Here we probe these modulations in long-lived equilibrium systems in both the stripe and plane-wave phases.

Our Letter is organized as follows: (i) we introduce the physics of SOBECs, (ii) we describe our experimental setup, (iii) we cross-check our Bragg measurements with established techniques, (iv) we demonstrate the coexistence of diagonal and off-diagonal order in the same system, and (v) we discuss the implications of these measurements on the issues of supersolidity in stripe-phase SOBECs.

SOBECs with Raman coupling.—We realized SOBECs described by the single-particle Hamiltonian

$$\hat{H}_0 = \frac{\hbar^2}{2m} [(q_x - k_R \hat{\sigma}_z)^2 + k_\perp^2] + \frac{\delta}{2} \hat{\sigma}_z + \frac{\Omega}{2} \hat{\sigma}_x \quad (1)$$

for particles of mass m . Here, δ and Ω describe Zeeman shifts from longitudinal and transverse fields, respectively, and the spin-orbit coupling (SOC) strength k_R defines the relevant energy scale $E_R = \hbar^2 k_R^2 / 2m$. $\hbar q_x$ is the quasi-momentum along \mathbf{e}_x , $\hbar k_\perp$ is the linear momentum in the $\mathbf{e}_y - \mathbf{e}_z$ plane, and $\hat{\sigma}_{x,y,z}$ are Pauli operators. The insets to Fig. 1(a) show the characteristic double-well dispersion

Published by the American Physical Society under the terms of the [Creative Commons Attribution 4.0 International license](https://creativecommons.org/licenses/by/4.0/). Further distribution of this work must maintain attribution to the author(s) and the published article's title, journal citation, and DOI.

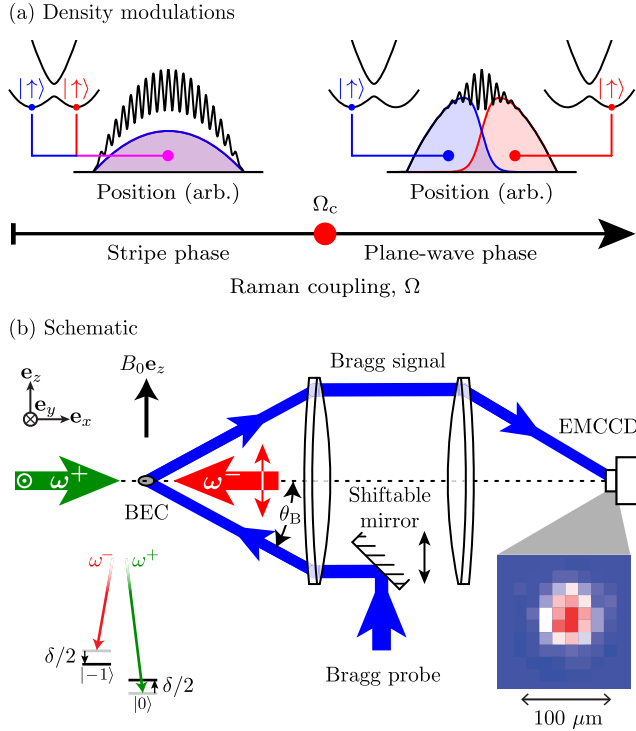


FIG. 1. Experimental concept and setup. (a) Schematic description of small- δ phase diagram with equal spin populations showing the stripe and plane-wave phases. The spatial distribution of the two spin-orbit-coupled spin states is marked in red and blue for $|\uparrow\rangle$ and $|\downarrow\rangle$, respectively, while the total density is in black. The insets depict the dispersion of these states. (b) Laser configuration for realizing SOC system with two-photon Raman transition and detecting scattered Bragg signal from the stripe phase. We choose a bias magnetic field $B_0 \approx 20$ G. The inset shows an example of diffracted Bragg signal as imaged by an EMCCD camera.

associated with SOC, with minima separated by approximately $2k_R$, and energy gap equal to Ω . In our experiments, we use two-photon Raman transitions to introduce the SOC term: the Raman laser wavelength determines the SOC strength $k_R = 2\pi/\lambda_R$; the Raman laser intensities determine Ω ; and the laser frequency differences imbue detuning δ to the SOC system [5,6].

We describe the two spin-components of our system by the spinor wave function $(\psi_\uparrow, \psi_\downarrow)^T$, where the mean-field interaction energy density is

$$\varepsilon = \left[\frac{c_0}{2} + \frac{c_2}{4} \right] [|\psi_\uparrow|^2 + |\psi_\downarrow|^2]^2 - \frac{c_2}{4} [|\psi_\uparrow|^4 - |\psi_\downarrow|^4] + \frac{c_2}{2} |\psi_\uparrow \psi_\downarrow|^2.$$

Here c_0 and c_2 describe the inter- and intraspin interaction parameters, respectively, and \bar{n} is the mean density. For dilute Bose gases (with chemical potential $\mu \ll E_R$), the impact of interactions can be parametrized in terms of a

scaled recoil energy $E'_R = E_R + \mu/4$; in this case, the spin mixed, stable ground-state stripe phase, exists in a very narrow range of parameters [5]: with δ between 0 and $c_2 \bar{n}/2$; and $|\Omega| < \Omega_c$, with the critical coupling strength $\Omega_c = 4E'_R \sqrt{-2c_2/c_0}$. As depicted in Fig. 1(a) (left), the stripe-phase density

$$\frac{n(x)}{\bar{n}} = 1 + \frac{\Omega}{4E'_R} \cos [k(\Omega)x + \phi]$$

is modulated with wave vector

$$\frac{k(\Omega)}{2k_R} = \left[1 - \left(\frac{\Omega}{4E'_R} \right)^2 \right]^{1/2}. \quad (2)$$

The phase ϕ describing the stripe's location [6,13] results from the preexisting phase difference between the two spin components along with the relative phase between the Raman laser beams. On the contrary, for the plane-wave phase ($|\Omega| > \Omega_c$) shown in Fig. 1(a) (right), density modulations are expected only within the domain wall separating the now polarized spin components.

Experimental setup.—We produced $N = 2.2(3) \times 10^5$ condensed ^{87}Rb atoms in a harmonic trap with frequencies $(f_x, f_y, f_z) = [(105, 67, 40)]$ Hz and chemical potential $\mu = [h \times 1.46(20)]$ kHz. Two Raman lasers, counter-propagating along \mathbf{e}_x , coupled the $|\downarrow\rangle \equiv |f=1, m_F=-1\rangle$ and $|\uparrow\rangle \equiv |f=1, m_F=0\rangle$ hyperfine levels of ^{87}Rb $5S_{1/2}$ electronic ground states. We used the tune-out wavelength [14] $\lambda_R = 790.034(7)$ nm for our Raman lasers which defined the single-photon recoil energy $E_R = h \times 3.678$ kHz and the scaled recoil energy $E'_R/E_R = 1.10(2)$ governing the stripe-phase physics.

We used optical Bragg scattering [15–17] to detect periodic density modulations. The Bragg probe laser, with wavelength $\lambda_B = 780.24$ nm, was ≈ 6.3 GHz red detuned from the $f=1 \rightarrow f'=0, 1, 2$ transition within the D_2 line [18]. This put the Bragg probe beam in the far-detuned limit with respect to the ≈ 6 MHz transition linewidth, the ≈ 10 MHz Zeeman shifts, and the ≈ 300 MHz excited state hyperfine structure. In this limit, the atomic susceptibility is almost entirely real and state independent. Figure 1(a) shows our experimental setup, with atoms located at the focus of a Keplerian imaging system aligned along \mathbf{e}_x . The Raman lasers propagated along \mathbf{e}_x and the Bragg probe had an incident angle θ_B with respect to the optical axes. A shiftable mirror in the back focal plane tuned θ_B from 80 to 280 mrad, allowing the detection of Bragg scattering from structures with period from about 391 to 405 nm; we used $\theta_B \approx 0.15$ rad in these experiments [19]. In ^{87}Rb , the interaction constants [24] are $(c_0, c_2) = (779, -3.61) \times 10^{-14}$ Hz cm³, so the stable ground-state stripe phase was present for $\Omega \lesssim 0.21 E_R$ and $-3.3 \text{ Hz} < \delta/h < 0 \text{ Hz}$.

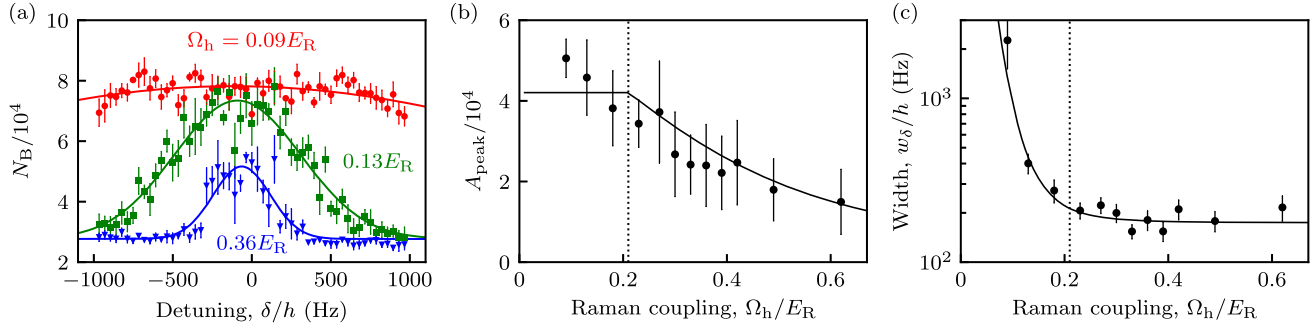


FIG. 2. Bragg-scattering as a function of Ω_h and δ . (a) $N_B(\delta)$ from a $t_B = 100 \mu\text{s}$ pulse for various coupling strengths Ω_h ; each data point is an average of more than four realizations. The solid curves depict Gaussian fits to the data from which the peak amplitude A_{peak} and width w_δ in (b) and (c) are derived. The increased background level as compared to Fig. 1 is from an increased overall atom number. In (b) and (c), the vertical dotted line marks the critical coupling strength at $\Omega_c = 0.21 E_R$, showing that the Bragg amplitude lacks a sharp feature at Ω_c , while the width drops rapidly leading up to Ω_c .

The Bragg diffracted signal, as shown in the inset of Fig. 1(b), was detected with an electron-multiplying charge-coupled device (EMCCD) camera. As described in Ref. [19], we first calibrated our Bragg signal using an optical lattice and found that the signal-to-noise ratio of one occurred for a fractional density modulation of $\eta = 0.06$, providing practical detection threshold.

We prepared our SOBECS from an initial BEC with equal superposition of spin $|\uparrow\rangle$ and $|\downarrow\rangle$ at a desired detuning δ and linearly increased Ω from 0 to Ω_h in 50 ms. We then allowed the system to equilibrate for a hold time t_h . At the transition from stripe to plane-wave phase at $\Omega_c \approx 0.21 E_R$, the expected density modulation contrast is just $\eta = 0.045$, just below our detection threshold. Inspired by Ref. [25], we rapidly ramped Ω to $\approx 7 E_R$ in 200 μs just prior to our Bragg measurement, increasing η to ≈ 0.85 (see Ref. [19]). This rapid ramp was slow compared to the $\approx 4 E_R$ energy spacing between the two branches of the SOC dispersion, but fast compared to the much slower many-body dynamics. In this system, the shortest many-body timescale is the $\gtrsim 2.5$ ms quarter period of our harmonic trap, followed by the ≈ 50 ms timescale for any significant evolution of spin structure [5,19]. As a result, this process simply magnified the amplitude of the SOC driven stripes wherever they were present in the system. We then turned the Raman lasers off and pulsed the Bragg laser with duration t_B ranging from 20 to 100 μs .

Validation of method.—We began by demonstrating our ability to maintain balanced spin mixtures very near $\delta = 0$ in the process of cross-checking our Bragg measurements against earlier time-of-flight experiments [5]. We characterized the transition from the stripe to plane-wave phase as a function of Raman coupling Ω_h and detuning δ . Figure 2(a) shows the number of photoelectrons N_B in our detection region as a function of δ at different values of Ω_h for a fixed hold time $t_h = 1$ s. We observe Bragg scattering in a narrow detuning window that decreases in width and amplitude as Ω_h increases.

Figure 2(b) quantifies the amplitude in terms of the peak height A_{peak} obtained from Gaussian fits to $N_B(\delta)$. We might expect the Bragg scattering amplitude to be constant in the stripe phase $\Omega_h < \Omega_c$ where the spin components mix and then to vanish in the plane-wave phase when the gas becomes locally polarized. However, even when different plane-wave regions phase separate, density modulations are present in the domain wall separating the different phases, allowing some Bragg scattering. The spin healing length $\xi_s/\xi = \sqrt{c_0/[-c_2(\Omega_h^2/\Omega_c^2 - 1)]}$ in terms of the conventional healing length $\xi = \hbar/\sqrt{2m\mu}$. ξ_s sets the domain wall size [5] and diverges at Ω_c . Figure 2(b) shows $A_{\text{peak}}(\Omega_h)$ rapidly falling with increasing coupling strength, consistent with the expected trend. The solid curve is a fit to our scattering model (derived from the above reasoning and developed in Ref. [19]) with the overall Bragg signal as the only free parameter. This model shows only qualitative agreement with data, a point we will return to shortly.

Figure 2(c) plots the Gaussian width w_δ . Even for $\Omega_h < \Omega_c$, a small detuning $\delta \neq 0$ that breaks the degeneracy of the two spin states can cause the initially spatially mixed states to relax into a polarized gas in the lower energy spin state: a plane-wave phase with no Bragg scattering. When $\Omega_h = 0$, there are no spin-changing processes, and the spatially mixed state is stable indefinitely, independent of δ . The width is thus large for small Ω_h (slower spin relaxation) and decreases as Ω_h increases (faster spin relaxation). The width has no marked feature at Ω_c and is well fit by a power law [5], here $a(\Omega_h/E_R)^{-4} + w_\infty$. This indicates that the process by which the spin population polarizes in the presence of detuning is dependent on the Raman coupling strength, but not the initial zero-detuning phase.

In all cases, the detuning window is far wider than the 3.3 Hz range of detuning where the stripe phase is thermodynamically stable. This is as expected: the time-scale for the spin populations to reach the expected equilibrium population can be in excess of several seconds

for small detunings (see Refs. [5,19] for a discussion of the equilibration timescale). In what follows, we focus on near-zero detunings that lie within this metastable region and where the physics is governed by Ω_h alone.

Spatial coherence.—Finally, we present our main observation demonstrating the spatial coherence of the SOBECs. Here we altered our measurement procedure to include a free evolution time t_{rev} following the turn-off of the Raman lasers but prior to the Bragg pulse. During this time, the different spin and momentum components that comprised the Raman dressed states underwent free evolution creating a matter-wave Talbot interferometer [17,26,27]. A coherent matter wave with wave vector k_R exhibits a coherence revival after a time period of $T_{\text{rev}} = h/8E_R = 34.0 \mu\text{s}$, during which time momentum components traveling with velocity $\pm 2\hbar k_R/m$ separated by a distance λ_R . Figure 3(a) schematically depicts this behavior: the left panel shows modulations in total density (black) and in each spin component (red and blue) at $t = 0$; the center panel shows that after $T_{\text{rev}}/2$ the modulation pattern in each spin component moved $\pm 1/4$ of the overall modulation period, yielding a flat density profile. The right panel shows the long-time behavior in which the spin components moved a distance comparable to the overall system size.

The periodic revivals in Fig. 3(b) occurred very near the $34 \mu\text{s}$ free-particle Talbot time, only about one-third of our earlier $100 \mu\text{s}$ Bragg pulse time. This indicates that all of our previous measurements inadvertently integrated over about three periods of collapse and revival. To resolve the Talbot signal, we largely mitigated this effect by reducing the pulse time to $t_B = 20 \mu\text{s}$ and averaging over at least four experimental realizations to account for the reduced signal present in each measurement.

Figure 3(c) shows N_B as a function of t_{rev} for a range of Ω_h , each constituting a single horizontal cut through Fig. 3(b). In Fig. 3(c), we observe damped oscillatory behavior that provides a lower bound to the coherence length of the system (other physical effects [17] may also cause the decay of $N_B(t_{\text{rev}})$). Our observations are complicated by the $20 \mu\text{s}$ Bragg pulse which is not short compared to the revival time. We modeled the integrated Bragg signal as a sinusoid with Gaussian decay [28] convolved with our Bragg pulse to obtain

$$N_B(t) = A_{\text{rev}} \int_t^{t+t_B} \frac{dt'}{t_B} \cos^2\left(\frac{\pi t'}{T_{\text{rev}}}\right) e^{-(t'/t_d)^2} + c, \quad (3)$$

as displayed by the solid curves in Fig. 3(c). Here $t_B = 20 \mu\text{s}$ is the Bragg pulse duration and the fitting parameters are revival amplitude A_{rev} , revival period T_{rev} , decay time t_d , and constant c .

Figures 3(d) and 3(e) show the revival amplitude A_{rev} and period T_{rev} as a function of coupling strength Ω_h . The amplitude A_{rev} gradually decreases above $\Omega_h > 0.21E_R$, which we attribute to the onset of phase separation and

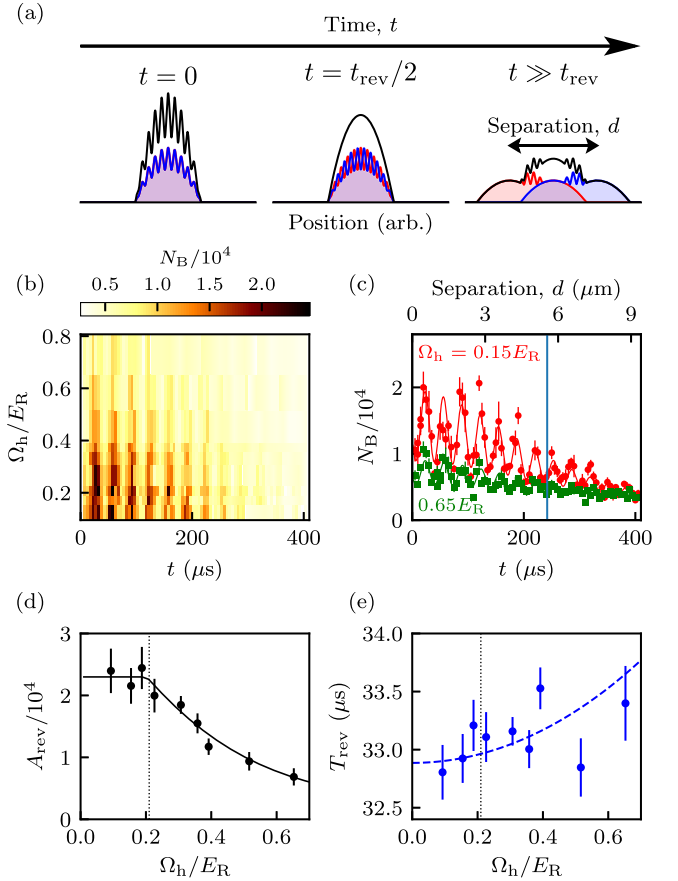


FIG. 3. Periodic revival of Bragg signal at $\delta = 0$ Hz. (a) Schematic representation of evolution of stripes during free evolution. The black, red, and blue curves depict total density, spin-up density, and spin-down density, respectively. (b) Observed Bragg counts N_B from a $t_B = 20 \mu\text{s}$ pulse as functions of (Ω_h, t) . (c) $N_B(t)$ for various coupling strength Ω_h , showing revivals characteristic of an atomic Talbot effect. The solid curves are joint fits of the model described in the text with shared parameters: decay time $t_d = 250 \mu\text{s}$ and background level $c = 3487$ counts. The vertical blue line depicts the separation equal to the calculated Thomas-Fermi radius. (d), (e) depict the amplitude A_{rev} and period T_{rev} obtained from fits to the data in (b). The vertical dotted lines show the predicted transition strength at Ω_c . The dashed blue curve indicates prediction for $T_{\text{rev}}(\Omega)$ shifted down by $1.1 \mu\text{s}$.

subsequent increasing separation between the two plane-wave components. The solid curve depicts the fit to the scattering model described in Ref. [19] with the overall scattering strength as the only free parameter, showing near perfect agreement with experiment. Allowing Ω_c to vary in the scattering model produces a value $\Omega_c = 0.20(1)$, also in agreement with our expectations. Figure 3(e) shows revival periods close to $T_{\text{rev}} = 33 \mu\text{s}$, just below the naive single-particle prediction. Our model in Eq. (2) predicts an increase in T_{rev} for larger Ω_h as the stripe wave vector $k(\Omega)$ falls. This increasing trend is plotted by the blue dashed curve; both this model and the null hypothesis are

consistent with the data. In addition, the energy scale E'_R in Eq. (2) was derived from a variational study of the stripe phase [13]; a similar energy scale—potentially different from E'_R —will be required within the domain wall and a proper variational study would be required to identify its exact value.

Last, the decay time $t_d = 250 \mu\text{s}$ was independent of Ω_h , indicating that the transition from the stripe phase to the plane-wave phase was not associated with any decrease in spatial coherence. During this $250 \mu\text{s}$, the interfering momentum states are separated by $5.8 \mu\text{m}$, comparable to the $R_{\text{TF}} = 5.5 \mu\text{m}$ Thomas-Fermi radius [shown by the vertical line in Fig. 3(c)]. We conclude that the system was fully coherent even in the phase-separated plane-wave phase.

Implications for supersolidity.—As has now been observed with dipolar atoms [29], a traditional supersolid is a phase of matter with two broken symmetries [30]: the broken gauge symmetry of a BEC (giving a superfluid phonon mode) and the broken translation symmetry of a lattice (giving a separate lattice-phonon mode). On one hand, we confirmed that diagonal order is present [8] and demonstrated that this coexists with off-diagonal order: a supersolid? On the other hand, a BEC in a shallow optical lattice has off-diagonal order, with density modulations (diagonal order) simply imprinted by the lattice potential [31]: not a supersolid.

With the Raman lasers off, our system is a two-component spinor BEC with two broken symmetries giving an overall phase (giving a superfluid phonon mode) and a relative phase between the spin components (giving a spin-wave mode); translational symmetry is unbroken: not a supersolid. Adding Raman coupling continuously connects this spinor phase to the stripe phase. For infinitesimal coupling, the modulation period [from Eq. (2)] is externally imposed by the Raman lasers, with a small shift that grows quadratically with Raman coupling. The spatial phase is set both by the relative phase between the Raman lasers and the preexisting relative phase between spin components. Similar to the lattice case, no new symmetries are broken and no new collective modes are created: not a supersolid? Although no new symmetries are broken, the spin-wave mode acquires an inertial contribution from the periodic density modulations inducing a gap at the edge of the associated Brillouin zone, as would be expected of a supersolid's lattice-phonon mode [7]. We conclude that this system shares some properties with conventional supersolids, but is best given its own name: the superstripe phase, as suggested in Ref. [7]. This is similar to the supersmectics proposed in Ref. [32] in which the mode structure of an optical cavity provides the substrate on which smectic correlations develop. The lattice-phonon mode remains undetected, and its observation would be a true smoking gun for observation of superstripes.

This work was partially supported by the Army Research Office's atomtronics Multidisciplinary University Research Initiative (MURI), the Air Force Office of Scientific Research's Quantum Matter MURI, the National Institute of Standards and Technology, and the National Science Foundation through the Physics Frontier Center at the Joint Quantum Institute (Award No. 1430094). We are grateful for the very thoughtful and detailed eleventh hour reading of our manuscript by Qiyu Liang and Alina Pineiro. We appreciate the temperature calibrations performed by Peter Zhou.

-
- [1] B. T. Matthias, H. Suhl, and E. Corenzwit, *Phys. Rev. Lett.* **1**, 449 (1958).
 - [2] Y. Pomeau and S. Rica, *Phys. Rev. Lett.* **72**, 2426 (1994).
 - [3] M. Dzero, K. Sun, V. Galitski, and P. Coleman, *Phys. Rev. Lett.* **104**, 106408 (2010).
 - [4] T. D. Stanescu and V. Galitski, *Phys. Rev. B* **75**, 125307 (2007).
 - [5] Y. J. Lin, K. Jimenez-Garcia, and I. B. Spielman, *Nature (London)* **471**, 83 (2011).
 - [6] T.-L. Ho and S. Zhang, *Phys. Rev. Lett.* **107**, 150403 (2011).
 - [7] Y. Li, G. I. Martone, L. P. Pitaevskii, and S. Stringari, *Phys. Rev. Lett.* **110**, 235302 (2013).
 - [8] J.-R. Li, J. Lee, W. Huang, S. Burchesky, B. Shteynas, F. c. Top, A. O. Jamison, and W. Ketterle, *Nature (London)* **543**, 91 (2017).
 - [9] J. Higbie and D. M. Stamper-Kurn, *Phys. Rev. A* **69**, 053605 (2004).
 - [10] T. D. Stanescu, B. Anderson, and V. Galitski, *Phys. Rev. A* **78**, 023616 (2008).
 - [11] C. Wang, C. Gao, C.-M. Jian, and H. Zhai, *Phys. Rev. Lett.* **105**, 160403 (2010).
 - [12] W. S. Bakr, J. I. Gillen, A. Peng, S. Fölling, and M. Greiner, *Nature (London)* **462**, 74 (2009).
 - [13] Y. Li, L. P. Pitaevskii, and S. Stringari, *Phys. Rev. Lett.* **108**, 225301 (2012).
 - [14] B. Arora, M. S. Safronova, and C. W. Clark, *Phys. Rev. A* **84**, 043401 (2011).
 - [15] M. Weidemüller, A. Hemmerich, A. Görlitz, T. Esslinger, and T. W. Hänsch, *Phys. Rev. Lett.* **75**, 4583 (1995).
 - [16] G. Birkel, M. Gatzke, I. H. Deutsch, S. L. Rolston, and W. D. Phillips, *Phys. Rev. Lett.* **75**, 2823 (1995).
 - [17] H. Miyake, G. A. Siviloglou, G. Puentes, D. E. Pritchard, W. Ketterle, and D. M. Weld, *Phys. Rev. Lett.* **107**, 175302 (2011).
 - [18] C. A. Müller, C. Miniatura, D. Wilkowski, R. Kaiser, and D. Delande, *Phys. Rev. A* **72**, 053405 (2005).
 - [19] See Supplemental Material at <http://link.aps.org/supplemental/10.1103/PhysRevLett.124.053605> for additional details, which includes Refs. [20–23].
 - [20] D. McKay and B. DeMarco, *New J. Phys.* **12**, 055013 (2010).
 - [21] N. Marzari, A. A. Mostofi, J. R. Yates, I. Souza, and D. Vanderbilt, *Rev. Mod. Phys.* **84**, 1419 (2012).

- [22] B. Gadway, D. Pertot, R. Reimann, M. G. Cohen, and D. Schneble, *Opt. Express* **17**, 19173 (2009).
- [23] W. Bao, D. Jaksch, and P. A. Markowich, *J. Comput. Phys.* **187**, 318 (2003).
- [24] A. Widera, F. Gerbier, S. Fölling, T. Gericke, O. Mandel, and I. Bloch, *New J. Phys.* **8**, 152 (2006).
- [25] R. A. Hart, P. M. Duarte, T.-L. Yang, X. Liu, T. Paiva, E. Khatami, R. T. Scalettar, N. Trivedi, D. A. Huse, and R. G. Hulet, *Nature (London)* **519**, 211 (2015).
- [26] H. F. Talbot Esq. F. R. S., *Philos. Mag. J. Sci.* **9**, 401 (1836).
- [27] B. Santra, C. Baals, R. Labouvie, A. B. Bhattacharjee, A. Pelster, and H. Ott, *Nat. Commun.* **8**, 15601 (2017).
- [28] We also considered exponential decay, but the overall χ^2 was increased by a factor of 4.
- [29] G. Natale, R. M. W. van Bijnen, A. Patscheider, D. Petter, M. J. Mark, L. Chomaz, and F. Ferlaino, *Phys. Rev. Lett.* **123**, 050402 (2019).
- [30] M. Boninsegni and N. V. Prokof'ev, *Rev. Mod. Phys.* **84**, 759 (2012).
- [31] M. Greiner, O. Mandel, T. Esslinger, T. W. Hansch, and I. Bloch, *Nature (London)* **415**, 39 (2002).
- [32] S. Gopalakrishnan, B. L. Lev, and P. M. Goldbart, *Phys. Rev. A* **82**, 043612 (2010).